Title

A Pressure-Sensitive, Repositionable Bioadhesive for Instant, Atraumatic Surgical Application on Internal Organs (Adv. Mater. 1/2025)

Journal

Advanced Materials, 37(1)

ISSN

0935-9648

Authors

Nam, Kum Seok

Kim, Yeji

Park, Geonho

et al.

Publication Date

2025

DOI

10.1002/adma.202570001

Peer reviewed

ADVANCED MATERIALS
www.advmat.de

A Pressure-Sensitive, Repositionable Bioadhesive for Instant, Atraumatic Surgical Application on Internal Organs

Kum Seok Nam, Yeji Kim, Geonho Park, Kiwook Hwang, Minyoung Kim, Jooyeun Chong, Jooik Jeon, Congqi Yang, Yung Hsiang Lu, Christian Paniccia, Jeongwon Choi, Dong Geun Kim, Haeseung Lee, Seung Won Oh, Sanha Kim, Jae-Wook Rhyu, Jiheong Kang, Jung Keun Hyun, Jeffrey M. Karp, Yuhan Lee, Hyunwoo Yuk,* and Seongjun Park**

Pressure-sensitive adhesives are widely utilized due to their instant and reversible adhesion to various dry substrates. Though offering intuitive and robust attachment of medical devices on skin, currently available clinical pressure-sensitive adhesives do not attach to internal organs, mainly due to the presence of interfacial water on the tissue surface that acts as a barrier to adhesion. In this work, a pressure-sensitive, repositionable bioadhesive (PSB) that adheres to internal organs by synergistically combining the characteristic viscoelastic properties of pressure-sensitive adhesives and the interfacial behavior of hydrogel bioadhesives, is introduced. Composed of a viscoelastic copolymer, the PSB absorbs interfacial water to enable instant adhesion on wet internal organs, such as the heart and lungs, and removal after use without causing any tissue damage. The PSB's capabilities in diverse on-demand surgical and analytical scenarios including tissue stabilization of soft organs and the integration of bioelectronic devices in rat and porcine models, are demonstrated.

1. Introduction

Pressure-sensitive adhesives are routinely used in household, industrial, and medical applications due to their distinct adhesive properties. These adhesives are designed to form substrate-independent, instant, and reversible attachments to diverse surfaces, leveraging their viscoelastic properties to facilitate physical interactions.[1–3] In addition, pressure-sensitive adhesives are extremely simple and intuitive to attach and detach from the attached substrate, allowing people to use them without any specific training or instructions. In the clinic, pressure-sensitive adhesives are used for a wide range of on-skin applications in the form of a medical

K. S. Nam, Y. Kim, K. Hwang, M. Kim, C. Yang, H. Lee, S. W. Oh, S. Park
Department of Bio and Brain Engineering
Korea Advanced Institute of Science and Technology (KAIST)
Daejeon 34141, Republic of Korea
E-mail: spark19@kaist.ac.kr

D. G. Kim, S. Kim, H. Yuk
Department of Mechanical Engineering
Korea Advanced Institute of Science and Technology (KAIST)
Daejeon 34141, Republic of Korea
E-mail: hyunwooyuk@kaist.ac.kr

G. Park, Y. H. Lu, C. Paniccia, J. Choi, J. M. Karp, Y. Lee
Department of Anesthesiology
Perioperative
and Pain Medicine
Center for Accelerated Medical Innovation & Center for Nanomedicine
Brigham and Women's Hospital
Harvard Medical School
Boston, MA 02115, USA
E-mail: ylee21@bwh.harvard.edu

G. Park
Department of Nanoengineering
University of California San Diego
La Jolla, CA 92093, USA

G. Park
Department of Chemical and Biomolecular Engineering
Korea Advanced Institute of Science and Technology (KAIST)
Daejeon 34141, Republic of Korea

J. Chong, J. Kang
Department of Material Science and Engineering
Korea Advanced Institute of Science and Technology (KAIST)
Daejeon 34141, Republic of Korea

J. Jeon, J. K. Hyun
Department of Nanobiomedical Science and BK21 NBM Global Research
Center for Regenerative Medicine
Dankook University
Cheonan 31116, Republic of Korea

J.-W. Rhyu
Department of Cardiovascular Surgery
College of Medicine
Dankook University
Cheonan 31116, Republic of Korea

J. Kang, S. Park
KAIST Institute for NanoCentury
Daejeon 34141, Republic of Korea

The ORCID identification number(s) for the author(s) of this article can be found under https://doi.org/10.1002/adma.202407116

DOI: 10.1002/adma.202407116

tape or an adhesive film that can instantly adhere to medical devices (e.g., intravenous catheters, electrocardiogram sensors, and defibrillators). By allowing easy repositioning and removal of surgical equipment and analytical devices, pressure-sensitive adhesives minimize tissue damage and enhance surgical adaptability compared to sutures or nonreversible medical glues (**Figure 1a**; and Table S1, Supporting Information), thereby reducing complications during complex surgical procedures.

Pressure-sensitive adhesives (PSAs) have been utilized in applications limited to skin or nonmedical surfaces due to their physical adhesion mechanism. On macroscopic length scales, a combination of soft and viscoelastic material properties enable bulk deformation and flow upon the application of light pressure, ensuring intimate contact with dry substrates for optimal and instant wetting.[1,4,5] At the interface, various physical interactions (van der Waals and mechanical interlocking) act to enable adhesion independent of surface chemistry for attachment to both hydrophilic and hydrophobic substrates. Upon detachment, these physical interactions can also be reversibly formed, enabling multiple uses if the adhesive surface is not blocked by any foreign material (e.g., dust). However, when pressure-sensitive adhesives are applied on a wet hydrophilic substrate, such as wet internal organs, water on the tissue surface acts as an interfacial barrier between the adhesive and tissue during application, resulting in low adhesion.[6] This barrier impedes the physical interactions between the adhesive and underlying tissues that are crucial for pressure-sensitive adhesion.

In contrast, wet tissue adhesives have faced obstacles in adhesion to hydrophobic medical equipment without prior surface activation. Many reported tissue adhesives are formulated on the basis of hydrophilic matrices and chemical interactions, restricting the surface chemistries to hydrophilic surfaces with tissue-specific moieties based on covalent (e.g., primary amine groups via carbodiimide crosslinking chemistry) and ionic bonds.[7–15] This has posed specific requirements of surface chemistry, casting limitations on the application of diverse surfaces without the conjugation of the corresponding functional groups on the bonding substrates (Table S1, Supporting Information).[16–22] For adhesion on diverse surfaces, a chemical functionalization step is needed prior to clinical use, resulting in poor shelf stability and time-consuming multistep application procedures with specialized equipment and reagents (e.g., ultraviolet (UV) light generator, specialized glue mixing syringes, photoinitiators).

In addition, many chemical interactions from covalent bonds are irreversible and impede repositioning due to tissue damage during removal. However, many surgical settings may require removal and potential repositioning of equipment and medical devices. To enable removal after use, reversible (single-cycle) and repositionable wet tissue adhesives have been developed with a variety of detachment processes, such as triggering solutions and UV light.[23–29] However, these detachment processes may face difficulty in practical use on dynamic organs (long detachment times, harsh detachment conditions) and cannot be repositioned on hydrophobic surfaces due to constraints on the surface chemistry (Table S2. Supporting Information).

In this work, we present a pressure-sensitive, repositionable bioadhesive (PSB) that can achieve repositionable adhesion on substrates without limitations to surface chemistry (both hydrophilic and hydrophobic surfaces) via a physical, pressure-sensitive adhesion mechanism. The PSB physically bonds to wet internal organs by absorbing interfacial water and subsequently adheres using its viscoelastic properties (Figure 1a). By enabling instant (<1s) adhesion, the PSB is highly suitable for application on dynamic internal organs, in which their physiological activity may shift the application site during the time required for adhesion formation. Furthermore, the PSB can integrate with pre-existing medical devices to act as a bridging material from surgical tools and medical devices to internal tissues (Figure 1b). The PSB demonstrates a combination of high repositionability (75 cycles) and immediate adhesion (<1s) without limitations to surface chemistry (Figure 1c,d). The repositionable adhesion can provide atraumatic detachment and reattachment on internal tissues, reducing the risk of potential tissue damage and further assisting the surgeon for in situ adaptable positioning during surgical procedures (Figure 1e).

2. Results

2.1. Design and Synthesis of the Pressure-Sensitive Bioadhesive

The PSB utilizes an amphiphilic block copolymer entanglement network composed of biocompatible polymers (Figure 1f). The hydrophilic polyethylene glycol (PEG) moiety was chosen to absorb the interfacial water between the adhesive and wet surfaces. Poly(glycerol sebacate) (PGS) was introduced as a hydrophobic backbone to tune the entanglement network.[30] To synthesize a pressure-sensitive adhesive, we optimized the viscoelasticity of the PSB's amphiphilic block copolymer by tuning the reaction time. We employed a highly scalable, two-step polycondensation reaction to form the entanglement network of the PSB (Figure S1, Supporting Information).[31] The synthesis and reaction progression of the crosslinked polymers were confirmed with nuclear magnetic resonance analysis and Fourier transform infrared spectroscopy (Figures S2–S4, Supporting Information). The PSB demonstrated a glass transition temperature of −56.3 °C, falling within the range of previously reported PSAs (i.e., −20 to −60 °C), and a shifting glass transition temperature indicative of crosslinking (Figure S5, Supporting Information).[32] Furthermore, the crosslinking density of the PSB was measured as 0.050 mol m^{-3} ± 0.001 mol m^{-3} and indicates a reduced crosslinking density in comparison with previously reported PGS elastomers.[30]

During the bonding phase of the PSB, the hydrophilic PEG moiety rapidly absorbs and removes interfacial water to facilitate direct physical contact on wet tissue surfaces (Figure 1g).[13,33] The viscoelasticity of the PSB then further promotes conformal contact with tissue surfaces by viscoelastic flow, maximizing physical bond formation (e.g., mechanical interlocking and van der Waals interactions). During the debonding phase, the PSB's toughness and viscoelastic nature enable interfacial detachment rather than cohesive failure and subsequent repositionable adhesion (Figure 1g).[34,35] Notably, the physical adhesion mechanism of the PSB allows repeated reapplication and repositioning to wet surfaces similar to the mechanism of pressure-sensitive adhesive on dry surfaces (Figure S6, Supporting Information).

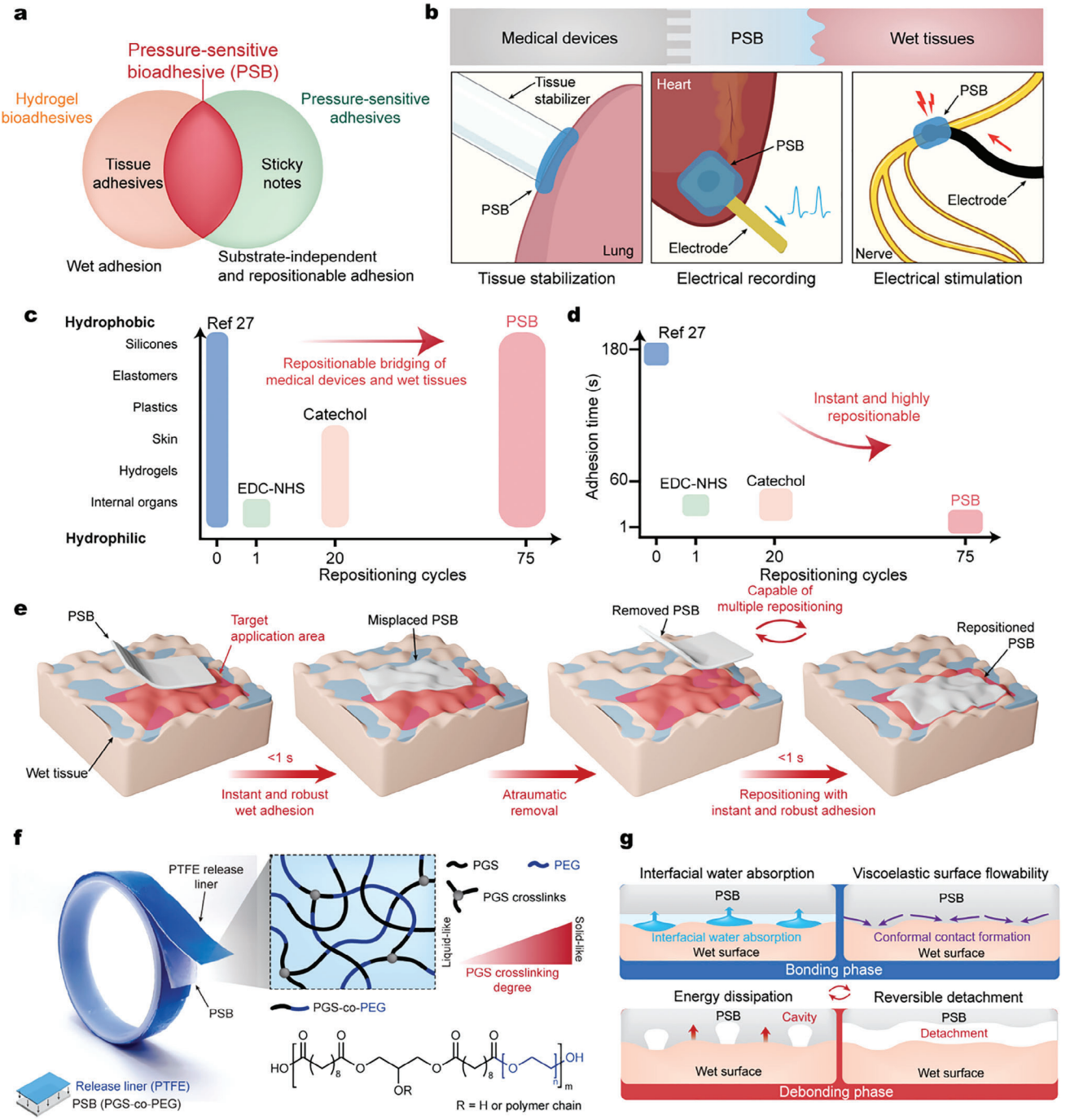

Figure 1. Concept and design of a pressure-sensitive bioadhesive. a) Schematic illustration for the concept of the PSB synergistically combining the advantages of tissue adhesives and pressure-sensitive adhesives for substrate-independent, instant, and repositionable adhesion. b) Schematic illustrations of the PSB enabling the near-instant, atraumatic adhesion between biomedical tools and wet internal tissues for applications, such as tissue stabilization and fault-tolerant bioelectronic interfacing. c) Range of applicable substrates without prior surface activation and repositioning cycles of the PSB in comparison with previous literature, including EDC-NHS (EDC, 1-ethyl-3-(3-dimethylaminopropyl) carbodiimide hydrochloride; NHS, N-Hydroxysuccinimide)[24] and catechol-based[29] adhesion mechanisms. EDC-NHS refers to carbodiimide crosslinking chemistry-based adhesives. d) Adhesion time and repositioning cycles of the PSB in comparison with previous literature. e) Schematic illustrations for independent, instant (<1s), and repositionable adhesion of the PSB. The repositionable adhesion of the PSB enables atraumatic removal and instant reapplication for fault tolerant applications. f) Image (left) and design (right) of the PSB. The hydrophilic PEG moiety absorbs interfacial water between the adhesive and wet surfaces. The crosslinked PGS enables optimized viscoelasticity. PGS, poly(glycerol sebacate). PEG, polyethylene glycol. PTFE, polytetrafluoroethylene. g) Schematic illustrations for the bonding and debonding phases of the PSB on a wet tissue surface. The bonding phase demonstrates a combination of interfacial water absorptions and viscoelastic flow for physical adhesion. During the debonding phase, the viscous component of the complex modulus acts as energy dissipation for adhesion hysteresis and reversible detachment. Figure 1b was created with BioRender.com.

2.2. Mechanism and Characterization of the Wet Viscoelastic Adhesion

Optimal viscoelasticity is a critical requirement for the PSB to be characterized as a pressure-sensitive adhesive.[2,34,36] As reaction time progresses, the crosslinking density of the PSB increases as seen by the increasing elastic modulus, and the macroscopic behavior of the amphiphilic block copolymer gradually transforms from viscous fluid to viscoelastic solid (**Figure 2**a; and Figure S7, Supporting Information).

To assess the bonding and debonding behavior of the PSB, the rheological properties were evaluated at frequencies corresponding to the bonding phase (corresponding to the complex modulus at 1 Hz) and the debonding phase (corresponding to the complex modulus at 100 Hz) (Figure 2b).[37] The optimized viscoelasticity of the PSB demonstrates a combination of good flowability for instant adhesion (viscous modulus higher than elastic modulus during the bonding phase) and elasticity for reversible adhesion (viscous modulus lower than elastic modulus during the debonding phase) in comparison to the viscous fluid and viscoelastic solid samples. In addition, the PSB satisfies the Dahlquist criterion (elastic modulus $< 10^5$ at 1 Hz), a critical parameter for pressure-sensitive adhesion to form robust yet reversible adhesion (Figure S8a, Supporting Information).[36,38] Optimal adhesion performance can be achieved at a loss factor range of ≈1.6–2.0 at 1 Hz (Figure S8b,c, Supporting Information). Due to the strict requirements in the complex modulus necessary for pressure-sensitive adhesion, only samples in this loss factor range are referred to as the PSB. Notably, the optimized PSB shows a tissue-like elastic modulus (≈100 Pa at 1 Hz). The low elastic modulus is expected to help mitigate potential tissue damage from elastic deformation during detachment.

To clearly visualize that the PSB is absorbing water at the adhesive-tissue interface, the PSB was adhered to a 2 wt% agarose hydrogel loaded with a fluorescent dye (Figure 2c). The interfacial water absorption was visualized by the transport of the dye from the bulk of the agarose hydrogel into the adhesive layers. As commercial PSAs cannot absorb the interfacial water, the transport of the fluorescent dye is trapped at the adhesive-hydrogel interface. In contrast, the PSB demonstrates transport of the fluorescent dye into the bulk material, demonstrating its ability to absorb interfacial water. In addition, to demonstrate that the adhesion mechanism of the PSB on wet tissues relies on a combination of water absorption and viscoelasticity, we compare the tensile adhesion (ASTM F2258-05) of the PSB with 1) a viscoelastic polymer without water absorption capabilities (i.e., pristine PGS without the hydrophilic PEG moiety, termed the viscoelastic PGS), 2) an elastomeric polymer with water absorption (elastomeric PGS-*co*-PEG), and 3) an elastomeric polymer with no water absorption capabilities (hydrophobic PGS). By introducing the hydrophilic PEG moiety to the PGS backbone, the water absorption capability increased to ≈9 wt% in both the PSB and elastomeric PGS-*co*-PEG, while the hydrophobic PGS polymer demonstrated no water absorption (Figure S9a, Supporting Information). The hydrophobic PGS polymer group had no adhesion to wet porcine skin during tensile testing, while the PSB demonstrated robust adhesion on wet porcine skin (Figure S9b, S9c, Supporting Information). Though elastomeric PGS-*co*-PEG absorbs water, elastomeric PGS-*co*-PEG also showed no adhesion to wet porcine skin due to its lack of viscous flowability. Furthermore, while viscoelastic PGS showed adhesion on dry porcine skin, there was a significant drop in adhesion for viscoelastic PGS when water was applied on the surface of the skin, unlike the PSB (Figure 2d). This indicates that the combination of viscoelasticity and interfacial water absorption was key for achieving robust, instant adhesion on wet surfaces.

To enable reversible adhesion cycles, the adhesive should be resistant to bulk damage from permanent deformation induced during its detachment process. We verify the self-healing capability of attaching two separate pieces of PSB and measuring the force required to separate the two pieces after self-healing (Figure 2e,f). The PSB demonstrates rapid self-healing characteristics to recover from bulk damages upon the application of light pressure, allowing it to maintain mechanical integrity and adhesion performance during multiple detachment-attachment cycles.

To investigate the debonding mechanisms of the optimized PSB with that of commercially available pressure-sensitive adhesives, the debonding process is monitored on both dry and wet surfaces (Figure 2g,h; and Video S1, Supporting Information). On dry surfaces, both VHB (i.e., commercially available pressure-sensitive adhesive) and PSB exhibit instant, robust, and reversible adhesion with a noticeable formation of cavitation and fibrillation, which are key characteristics of pressure-sensitive adhesives during the debonding process.[39] In contrast, VHB shows virtually no adhesion on wet surfaces, whereas the PSB provides nearly the same debonding characteristics as on the dry surface.

The PSB harnesses its distinct adhesive properties on internal organs. Application on an ex vivo porcine heart further demonstrates the robust attachment and atraumatic reattachment of the PSB in comparison with commercial and clinical pressure-sensitive adhesives (**Figure 3**a–c; and Figure S10 and Video S2, Supporting Information). To verify the instant and repositionable adhesion of the PSB, in comparison with commercial (e.g., VHB and FlexSeal) and clinical (e.g., Transpore and Micropore) pressure-sensitive adhesives on hydrophilic substrates with a cyclic tensile test (Figure 3d). The PSB demonstrates robust adhesion to both wet lung and heart tissue on five adhesive cycles in comparison to commercial and clinical pressure-sensitive adhesives (Figure 3e,f). While commercially available pressure-sensitive adhesives also exhibit consistent tensile strength and adhesion energy across test cycles, the tensile strength (2 kPa for VHB vs 18 kPa for the PSB) and adhesion energy (0.19 J m^{-2} for VHB vs 97 J m^{-2} for the PSB) of the PSB were over an order higher than VHB on wet porcine skin. The relatively low adhesive energy in lung and heart tissue, in comparison to skin tissue, results from the high energy dissipation and elongation in the tissue samples during testing. Furthermore, the PSB enables adhesion on blood-covered porcine skin (7.8 kPa) in comparison with VHB (2 kPa) to enable attachment on blood-covered tissues (Figure S11, Supporting Information). The PSB further demonstrates robust adhesion in semiwet environments (i.e., when the tissue is exposed to air) for up to 25 cycles on porcine skin in comparison with VHB (Figure S12, Supporting Information). To test the durability of the PSB, additional cyclic adhesion tests in semiwet environments were conducted on porcine skin. The PSB demonstrated stable adhesion for 1 h, displaying stable

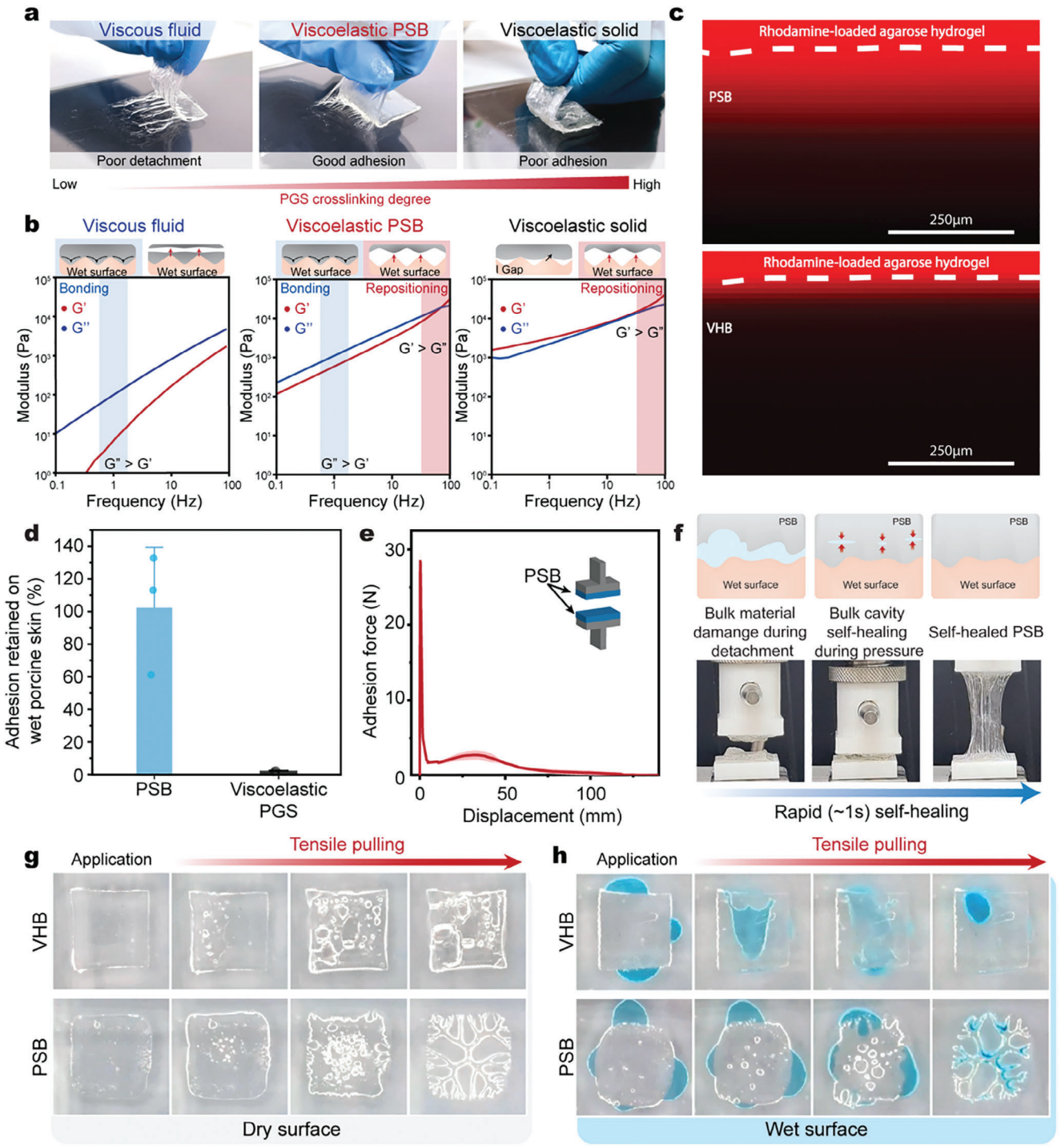

Figure 2. Adhesion mechanism of the PSB on internal organs via viscoelastic flow and interfacial water absorption. a) Images of the PSB with different complex moduli exhibiting viscous fluid (left, reaction time ≈70 h), viscoelastic PSB (middle, reaction time ≈76 h), and viscoelastic solid (right, reaction time %100 h) like behaviors. b) Change in viscoelastic behavior (shown through elastic modulus (G') and viscous modulus (G'')) during the reaction progression of the PSB. Frequency ranges corresponding to the bonding (blue, ≈1 Hz) and debonding (red, ≈100 Hz) behaviors in the viscous fluid state (left), viscoelastic PSB (middle), and viscoelastic solid state (right) are shaded. c) Interfacial water absorption of the PSB on wet hydrogel surfaces. Cross-sectional fluorescent image between 2 wt% agarose hydrogel and the PSB (top) in comparison with VHB (bottom). The dashed lines indicate the interface between the agarose hydrogel and the PSB or VHB. d) Tensile adhesion retained on wet porcine skin with reference to dry porcine skin for PSB and viscoelastic PGS. e) Self-healing stress–strain graph of two pristine PSB pieces after pressing for 5 s. The curve and shaded area represent the mean and standard deviation respectively ($n = 3$). f) Schematic and photos of robust, rapid self-healing process of two separate PSB pieces. g) Images of the VHB (top) and the PSB (bottom) application and detachment process on a dry glass surface. h) Images of the VHB (top) and the PSB (bottom) application and detachment process on a wet glass surface. Values in (d) represent the mean and the standard deviation ($n = \approx 3–6$).

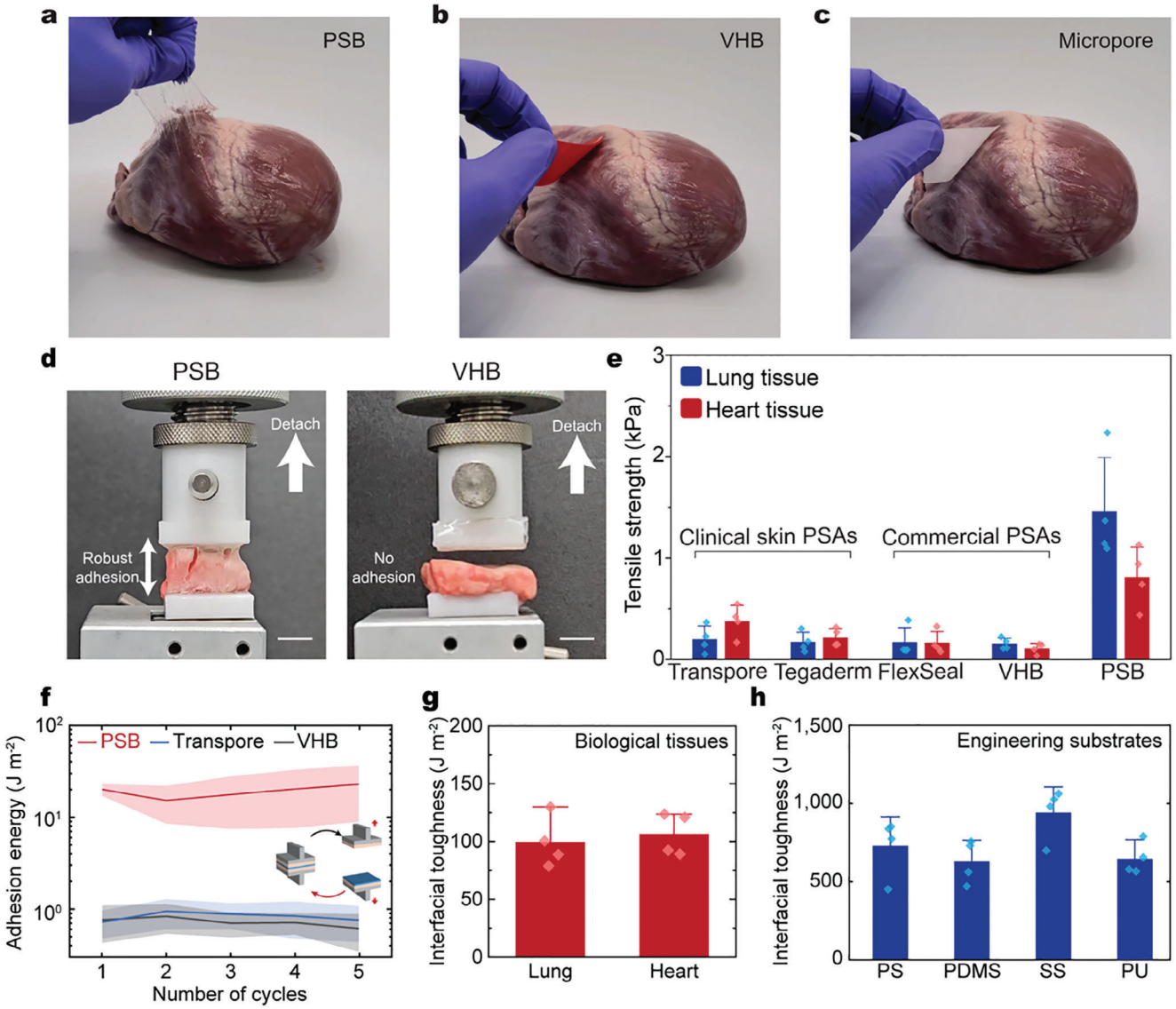

Figure 3. Adhesive properties of the PSB for substrate-independent, instant, and repositionable adhesion on internal organs. a–c) Photographic comparison of PSB and commercial pressure-sensitive adhesives on an ex vivo porcine heart. Image of robust adhesion on a porcine heart with a) PSB. Images of low adhesion on a porcine heart with b) VHB and c) Micropore. d) Images of the robust adhesion of PSB (left) on lung tissue in comparison to the low adhesion of VHB (right). e) Comparison of tensile strength with PSB and commercial and clinical pressure sensitive adhesives on lung and heart tissues. f) Cyclic adhesion of the PSB in comparison with commercial and clinical pressure sensitive adhesives on lung tissue. g) Interfacial toughness of the PSB on various biological tissues. h) Interfacial toughness of the PSB on various engineering substrates (polystyrene – PS, polydimethylsiloxane – PDMS, stainless steel – SS, polyurethane – PU). Values in (e)–(h) represent the mean and the standard deviation ($n = 4$ for (e)–(h)).

adhesion for 75 cycles on porcine skin in semiwet environments (Figure S13, Supporting Information). To further test the effects of water absorption on cyclic adhesion as the PSB swells, underwater adhesion tests were conducted (Figure S14, Supporting Information). As the PSB swells, peak tensile strength decreases due to the presence of excess water and reaches an equilibrium at 50% of the tensile strength of the initial adhesion cycle.

To verify the substrate-independent and instant adhesion of the PSB, 180° peel tests (ASTM F2256-05) were conducted on diverse medical substrates and internal organs. Owing to the physical bonding mechanism, the PSB achieves instant and robust adhesion to diverse hydrophilic and hydrophobic substrates, such as internal organs (interfacial toughness over 110 J m^{-2} for heart; 100 J m^{-2} for lung; 380 J m^{-2} for skin) and engineering solids commonly used in medical devices (interfacial toughness over 720 J m^{-2} for polystyrene; 630 J m^{-2} for polydimethylsiloxane; 940 J m^{-2} for stainless steel; 640 J m^{-2} for polyurethane) (Figure 3g,h; and Figure S15, Supporting Information). This allows the use of diverse backing materials, including stretchable (styrene-ethylene-butylene-styrene (SEBS) and Ecoflex), flexible (polyurethane), and stiff (polycarbonate) substrates (Figure S16, Supporting Information). Interfacial failure was validated with visual inspection and measurement of PSB tensile toughness values (Figure S17, Supporting Information). Notably, the

interfacial adhesion of the PSB saturated as low applied pressure and pressing times during peel testing (Figure S18, Supporting Information). This is seen to occur due to the low modulus of the PSB, in combination with the conformal contact induced by its good flowability.[40–41]

The synthesized PSB enables versatile fabrication into various forms, including single-sided or double-sided tapes, depending on the configuration of the application (Figure S19, Supporting Information). When the PSB is utilized in a single-sided configuration or double-sided configuration, it is subsequently referred to as the sPSB or dPSB, respectively.

2.3. Surgical Tissue Stabilization on Ultrasoft Organs

Clinical tissue stabilizers (e.g., Octopus Tissue Stabilizers, Medtronic) have been widely utilized for the mechanical stabilization of dynamically moving tissues (e.g., heart and lungs), allowing surgeons to operate on a stable, localized area without needing to stop the moving organ. During the tissue stabilization of internal tissues, vacuum suction is utilized to mechanically stabilize tissue (**Figure 4**a). The suction interface may be susceptible to detachments due to the mechanical mismatch between the tissue and the vacuum hose, making an interfacing adhesive beneficial in mechanically bridging the tissue (Figure 4b). Moreover, the strong suction pressure required during suction or gripping force applied by forceps often results in tissue damage on soft internal organs, such as the lungs.[42]

The dPSB's unique adhesive properties for substrate-independent, instant, and reversible adhesion enables three key functionalities as an interfacing adhesive in tissue stabilization: 1) Adhesion to bridge diverse surfaces including tissue stabilization devices and tissues, 2) instant adhesion on dynamic internal organs, and 3) on-demand atraumatic repositioning for tissue manipulation (Figure 4c). The dPSB demonstrates substrate-independent adhesion capable of stabilizing a rodent lung during respiration (Figure 4d). We compare the tissue stabilization of the dPSB by measuring the negative pressure on the suction tubing with and without the dPSB at the same suction pressure (Figure 4e; and Video S3, Supporting Information). The integration of the dPSB at the distal end of the tissue stabilizer significantly improves stabilizing pressure and enables instant attachment to the lung during respiratory movements. While higher suction pressure may mitigate such problems, this approach is undesirable for soft and fragile organs, such as the lungs, due to associated tissue damage and potential post-surgical complications.[43,44] Furthermore, the integration of the dPSB acts as an atraumatic interface by reducing the minimum pressure required for lung stabilization and enabling atraumatic detachment and subsequent reattachment (Figure 4f).

Prior to application on internal organs, we evaluated the in vitro and in vivo biocompatibility of the PSB. An in vitro LIVE/DEAD assay based on human embryonic kidney cells (HEK 293) and mouse embryonic fibroblast (3T3) cells show that the cytotoxicity of the PSB is comparable to that of the control group (Figure S20, Supporting Information). Subsequently, the PSB was implanted in the rat dorsal subcutaneous and epidermal implantation for 7 days. H&E staining data and lesion analysis conducted by a blinded histopathologist showed that the subcutaneously-implanted PSB-SEBS induced only a mild inflammatory reaction with mild inflammatory cell infiltration and fibrosis after 7 days, comparable to that of the control group (SEBS) (Figure 4g,h; and Figure S21, Supporting Information). During epidermal biocompatibility testing, the PSB with Ecoflex backing and the control group (Ecoflex) were applied on the dorsal epidermis. Evaluation of epidermal biocompatibility by a blinded histopathologist demonstrates that both groups do not exhibit observable signs of inflammation, through analysis on the epidermal thickness, inflammatory cell infiltration and fibrosis of the surrounding tissue (Figures S22–S23, Supporting Information).

The PSB further demonstrated hydrolytic biodegradation with 75% of its mass degraded within 48 h (Figure S24, Supporting Information). The biocompatibility of the biodegraded PSB was further validated through in vitro cell viability (Figure S20, Supporting Information) and in vivo subcutaneous implantation (Figure 4i). When only the PSB is implanted, the PSB exhibits negligible foreign body response due to its biocompatibility, fast biodegradation, and tissue-like mechanical properties (Figure 4i).

2.4. Fault-Tolerant Bioelectronic Interfacing on Dynamic Organs

To demonstrate in situ adaptable integration of implantable electrodes for bioelectronic stimulation, the sPSB was utilized to integrate an electrode on a rat sciatic nerve in vivo (**Figure 5**a). The sPSB enables the probing of multiple stimulation sites for precise placement with quick, atraumatic removal upon the end of the procedure. Enabled by the atraumatic and repositionable adhesion of the sPSB, the same stimulation electrode can be utilized to probe the transitions between upward- and downward-evoked hindlimb movements by repositioning the electrode to various locations on the sciatic nerve (Figure 5b).

To demonstrate fault-tolerant integration of implantable electrodes for bioelectronic sensing, the sPSB is utilized to reposition an electrode on rat left ventricular epicardial tissue in vivo (Figure S25a, Supporting Information). Upon the initial application of the epicardial electrode, the recorded electrocardiogram (ECG) does not display distinct left ventricular ECG signals due to the dynamic movements of the heart and subsequent misplacement of the electrode (Figure S25b, Supporting Information). The sPSB allows repeated atraumatic detachment and repositioning of the electrode to the epicardial tissue until the ECG waveform with a distinct left ventricular QRS complex, corresponding to standard 12-lead ECG signals, is achieved (Figure S25b,c, Supporting Information).[45]

We further demonstrate the applicability of sPSB-enabled applications in a large-animal porcine model (Figure 5c,d, Supporting Information). An epicardial electrode was integrated into a porcine heart in vivo by the sPSB and repeatedly repositioned until the measured ECG waveform with the targeted left ventricular QRS complex was achieved (Figure 5e). The integrated electrode by the sPSB exhibited stable adhesion and recording capability under the dynamic motions of the heart (Figure 5f). We also demonstrate rapid and atraumatic repositioning of the sPSB to soft and fragile organs, such as the porcine lungs (Figure 5g). The sPSB's capability to effectively integrate

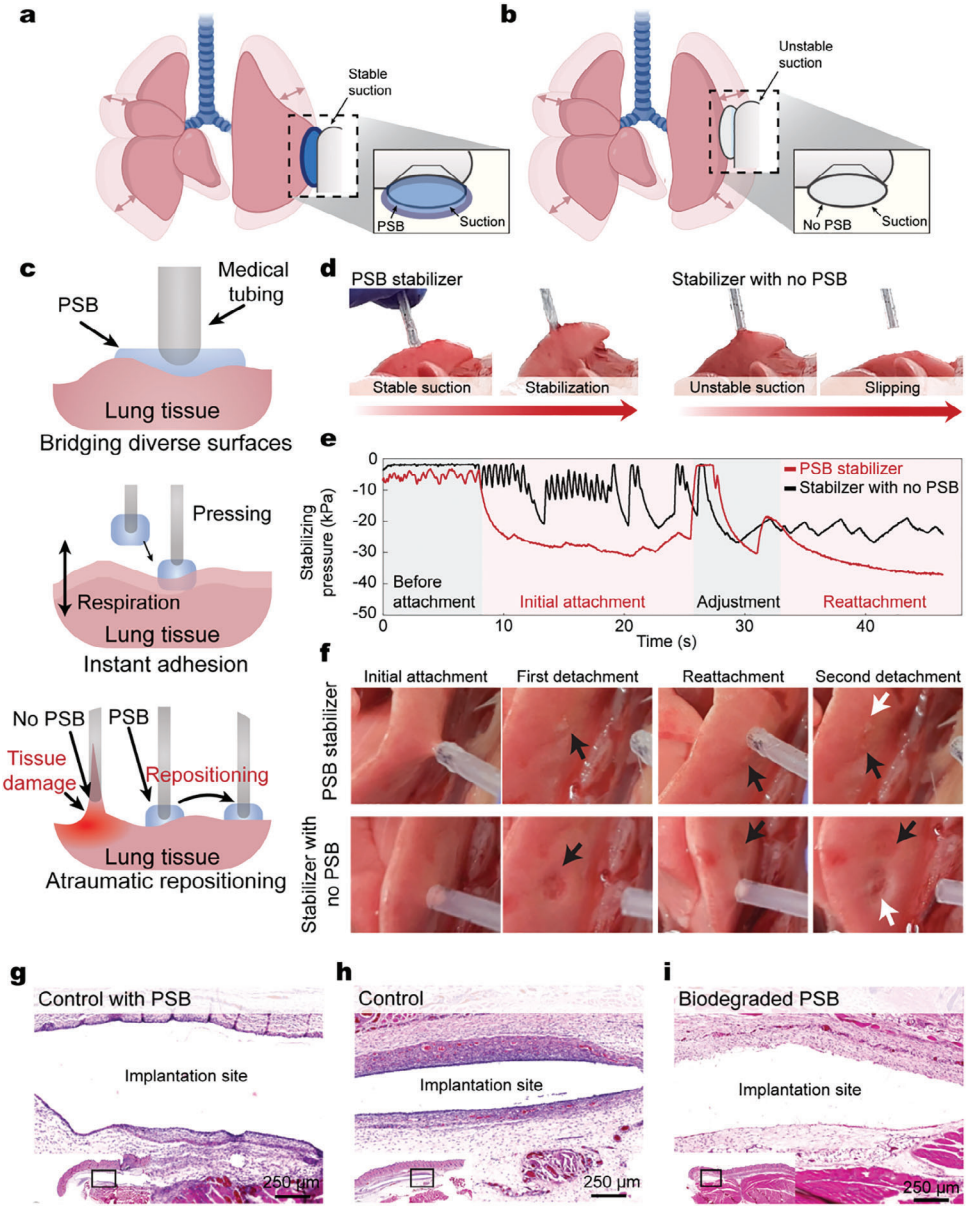

Figure 4. Atraumatic surgical tissue stabilization of dynamic internal organs. a,b) Schematic illustrations on the challenges of tissue stabilization a) with and b) without the application of the PSB. c) Schematic illustrations of functional effects of the PSB for use as in tissue stabilizing applications. d) Image comparison of tissue stabilizers on lung tissue with (left) and without (right) the PSB. e) Comparison of stabilizing pressure with and without the PSB during attachment and reattachment. f) Photos of minimal tissue damage with (top row) the PSB during tissue stabilization. Photos of tissue damage without (bottom row) the PSB during tissue stabilization. g–i) Representative histological images stained with hematoxylin and eosin (H&E) for the g) PSB with SEBS backing, h) a control SEBS backing, and the i) biodegraded PSB after 1 week of subcutaneous implantation for the evaluation of in vivo biocompatibility. SEBS, Styrene-ethylene-butylene-styrene. Figure 4a,b was created with BioRender.com.

and atraumatically reposition implantable devices on delicate organs allows in situ adaptive monitoring of strain changes in dynamic organs (Figure 5g,h). A custom-made strain sensor was integrated to a porcine lung by the sPSB and subsequently repositioned to different locations to obtain high-fidelity monitoring of lung inflation and deflation at various preset inhalation rates and locations without causing any tissue damage or use of new devices (Figure 5i; and Figures S26–S27, Supporting Information).

3. Discussion and Conclusion

Clinical pressure-sensitive adhesives are typically made from polymers like acrylics and styrene block copolymers.[2] When these polymers are crosslinked, they form an entangled network with viscoelastic properties, which can be measured by the complex modulus, including its elastic and viscous components. When light pressure is applied, if the elastic modulus of the viscoelastic polymer falls below the Dahlquist criterion, the

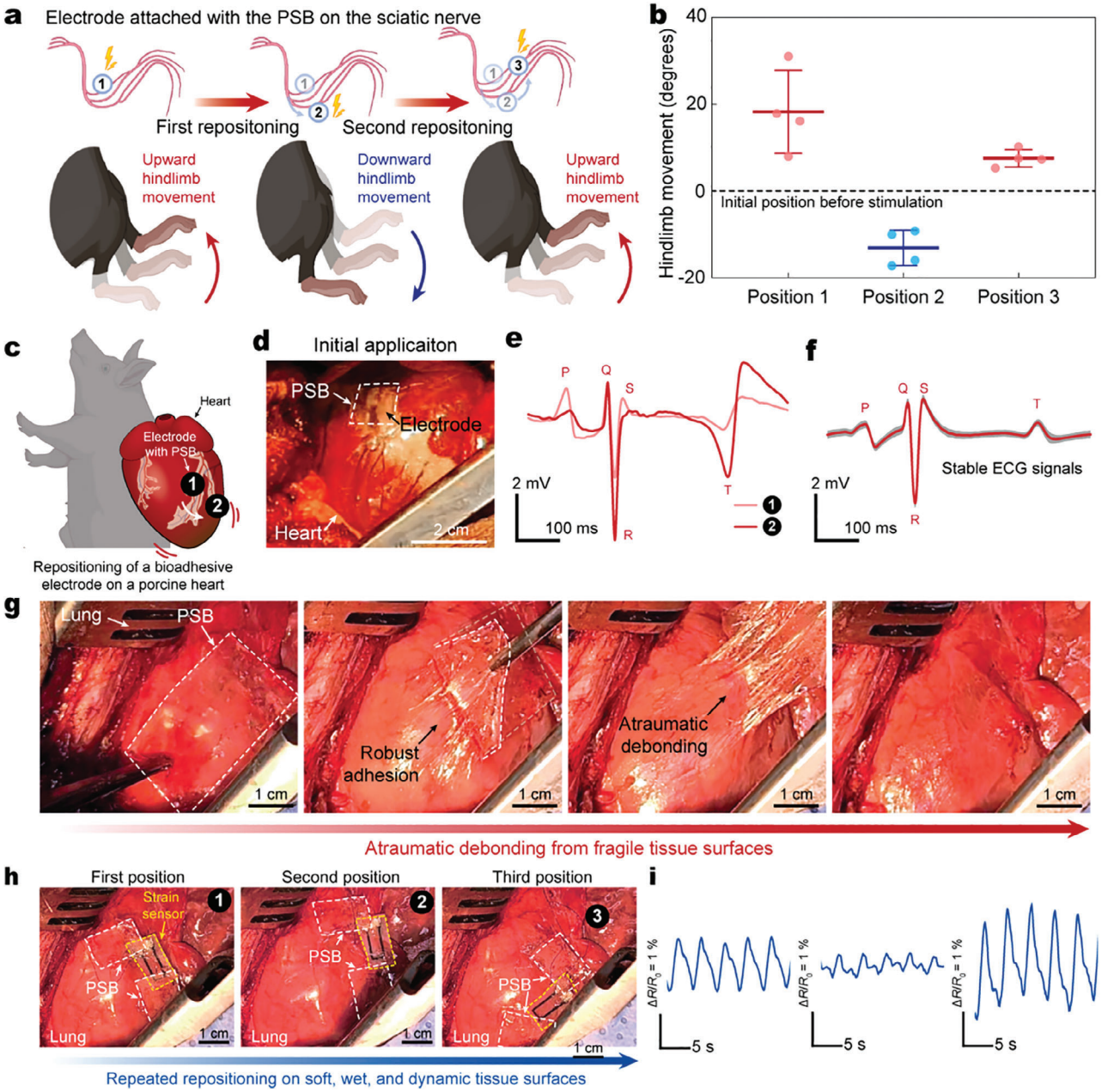

Figure 5. Fault-tolerant PSB-assisted bioelectronic interfaces for in vivo recording and sensing in rat and porcine models. a) Schematic illustrations for the PSB-assisted integration and repositioning of an electrode on the sciatic nerve for stimulation of the hindlimb. b) Measured hindlimb movements after stimulation by the electrode attached to different locations on the sciatic nerve by the PSB. c,d) c) Schematic illustration and d) image for PSB-assisted integration and repositioning of an electrode on the epicardial surface for the measurement of electrocardiogram (ECG) signals. e) Recorded ECG signals on the porcine heart during (1) initial application and (2) after repositioning. f) Average recorded ECG signals on the porcine heart for 10 min. The standard deviation of the signal is marked in gray. g) Snapshots of the fault-tolerant application of the PSB on the surface of the porcine lung. h) Representative images of the electrode integrated to the lung surface by the PSB in different locations after the first (left), second (middle), and final application (right). i) Measured impedance of the strain sensor during ventilator breathing movements on the first (left), second (middle), and final (right) applications. Values in (b) represent the mean and the standard deviation ($n = 4$). Figure 5a,c was created with BioRender.com.

polymers deform and make conformal contact with the target surface. For effective and reversible adhesion, the viscous modulus of the adhesive should be comparable to its elastic modulus. This balance in the complex modulus allows for instant and repositionable adhesion to a variety of dry surfaces, including medical devices and skin.[47]

While these clinical pressure-sensitive adhesives can adhere to hydrophobic tissues with low water content (≈15% – 30%), they cannot adhere to wet hydrophilic tissues, such as internal organs,

due to their high-water content (e.g., ≈83% water composition for lung and ≈74% for heart).[47–48] In addition, the surfaces of internal organs are constantly perfused with liquids from the bulk of the organ. Subsequently, a layer of water exists at the adhesive-organ interface, which has been shown to act as a critical barrier for forming adhesive interactions.

In this work, we developed the PSB to introduce the unique advantages of pressure-sensitive adhesives to wet internal organs by materials design, optimization, and characterizations. Unlike many bioadhesives that require specific surface chemistries or compositions to achieve wet adhesion, the PSB offers substrate-independent, instant, and reversible adhesion for surgical application.[4,13,27] The distinct adhesive performance of the PSB makes it an ideal material for bridging internal organs and surgical equipment.

We demonstrate two key applications of the PSB's unique adhesion mechanism for atraumatic tissue stabilization and fault-tolerant integration of bioelectronic interfacing on dynamic organs in both small and large animal models. When formulated as a single-sided tape, the PSB is composed of a bilayer structure by attaching any backing material to the PSB (e.g., polycarbonate, Ecoflex). The backing layer acts as a protective layer, covering the other side of the PSB. This plays a two-part role. It prevents indiscriminate adhesion to other internal organs or surgical tools, and it further allows for the application of pressure on top of the backing layer. When utilized as a double-sided tape, the PSB is able to act as an interfacing material between surgical tools and internal tissues to enable enhanced mechanical stability during interactions with internal organs. We envision that the PSB may enable new opportunities not only for the integration of implantable devices to the human body but also for clinical uses and improved patient care.[46] By acting as a bridge between medical devices and wet biological tissues, the sPSB can be utilized to attach commercial medical electrodes without prior preparation or surface functionalization for high-performance electrode arrays.

The main contribution of this work lies in the development of a mechanism for pressure-sensitive adhesion on wet internal organs. Through a combination of viscoelastic material properties and interfacial water absorption, the PSB demonstrates substrate-independent, instant, and repositionable adhesion for the first time on internal tissues, in comparison with previously reported PGS-co-PEG polymers in biomedical applications.[49] In order to target transient surgical applications, we have utilized the physical adhesion mechanism of pressure-sensitive adhesives, but through additional tuning of the complex modulus and integration of chemical adhesion, we foresee that the applications of the PSB can be extended to long-term surgical applications, such as surgical sealants and wound healing. Furthermore, the PSB adhesion mechanism will act as a design principle for future pressure-sensitive bioadhesives that aim to attach to internal organs.

The adhesive characteristics of the PSB demonstrate high utility in surgical and bioelectronic applications that interface with highly dynamic organs, such as tissue stabilization and fault-tolerant adhesion during bioelectronic interfacing. Due to the highly wet, soft, and dynamic nature of internal organs, the precise integration of implantable devices and surgical tools on target tissues has a risk of misplacement that requires repositioning or reapplication of the device to ensure desired functionality, especially in minimally invasive surgical settings for probing organs, such as the heart and sciatic nerve. These applications can range from epicardial recording for the identification of arrhythmias to deepening the understanding of mechanistic physiology in epicardial pacing and electrical stimulation of peripheral nerves for surgical placement of stimulators during open nerve surgery.[50–52]

The PSB demonstrates promising clinical applications during the immediate integration with medical devices possessing diverse surface chemistries. The soft tissue-like mechanical properties, in combination with its biocompatibility and biodegradability, will further allow atraumatic repositioning and minimal foreign body response if left inside the body after application. The PSB will not only provide an enabling tool for a wide range of biomedical and clinical applications, but also offer a basis for future developments in clinical translation.

4. Experimental Section

PGS-co-PEG and PGS Synthesis: The PGS-*co*-PEG was synthesized by a two-step polycondensation reaction. The first step involved the condensation polymerization of sebacic acid (133 mM, Sigma-Aldrich) and 1000 PEG (33 mM, Sigma-Aldrich) at 130 °C under a nitrogen atmosphere for 8 h, followed by the reaction under a vacuum of 50 mTorr for 16 h. The reaction was conducted in a heating mantle and the vacuum was fit to the reactor vessel with a screw cap containing hose connectors. In the second step, glycerol (67 mM, Sigma-Aldrich) was added, and the reaction was continued at 130 °C under the flow of nitrogen for 8 h followed by the reaction under a vacuum of 50 mTorr for 60 – 100 h. The reaction was terminated when the PGS-*co*-PEG reached a specified rheological value which corresponded to the reaction time of ≈75 – 90 h (0 h is set when the vacuum is started in the second step of the condensation reaction). PGS was synthesized in a one-step condensation reaction with sebacic acid and glycerol in a 1:1 molar ratio.

PSB Preparation: The PSB was prepared by removing the synthesized PGS-*co*-PEG from the reactor container and placing it on top of a backing material (0.125 mm thick polycarbonate; CT301303, Goodfellow). Polytetrafluoroethylene (PTFE, 0.1 mm thick; FP301300, Goodfellow) was then placed on top of the PGS-*co*-PEG as a release liner. To create a flat and uniform PSB, the PSB was pressed under 10 MPa at 120 °C by using a hot press (QM900L, QMESYS) for 10 min and cooled in a freezer (−20 °C). During the hot press procedure, 1 mm thick spacers were utilized to control the final thickness of the PSB. Samples were cut to sizes of 2.5 cm × 4 cm for 180° peel tests and 2.5 cm × 2.5 cm for cyclic tensile tests. The prepared PSB were stored with desiccants at −20 °C before use.

Rheological Characterization: For rheological characterization of the PSB, frequency sweep tests (0.1 – 100 Hz, 0.1% strain) were conducted with a rheometer (Anton Paar MCR302, 25 mm parallel plate geometry). The temperature was set to 37 °C and held for 2 min to emulate biological conditions. For tack adhesion tests, a 8 mm parallel plate probe was pressed for 1 s and pulled upward at 10 mm s^{-1}.

Chemical Characterizations: Attenuated total reflection Fourier transform infrared (ATR-FTIR) spectra of the PSB were scanned with a spectrometer (Nicolet iS50, Thermo Fischer) in the range of 400 – 4000 cm^{-1} with a resolution of 4 cm^{-1}. The spectra were acquired with 16 scans. Proton nuclear magnetic resonance (^{1}H NMR) spectroscopy was performed with a spectrometer (AVHD-400, Bruker) at 298 K. The PSB was dissolved in deuterated chloroform ($CDCl_3$) and the chemical shift was referenced to δ 7.24 ppm. The molar ratio between PEG and PGS in the PSB was calculated from the quantitative peak integration of methylene moiety of PEG at δ 1.30, 1.62, and 2.35 ppm and methylene moiety of sebacate at δ 3.64 ppm. Differential scanning calorimetry was conducted after nitrogen purging at a scan rate of 10 °C per minute from −100 to 200 °C.

Crosslinking density was calculated through the mechanical modulus as shown below[53]

$$\text{Crosslinking density} = \frac{E}{3RT} \quad (1)$$

where E represents the Young's modulus, $R = 8.314$ J mol^{-1} K^{-1}, and $T = 296.15$ K. Young's modulus values were measured at 371 Pa ± 8 Pa ($n = 3$).

Ex Vivo Tissue Preparation: Freshly harvested porcine skin and lung tissue were purchased from a local slaughterhouse in Daejeon. Porcine skin samples were cut into sizes of 2.5 cm × 4 cm for 180° peel tests and 2.5 cm × 2.5 cm for cyclic tensile tests. A polymethylmethacrylate (PMMA) film was attached to the fatty side of porcine skin with cyanoacrylate glue (Loctite). Porcine skin samples were covered with saline-soaked tissues and stored at −20 °C before use. Before mechanical testing, tissue samples were thawed and cleaned with 70% isopropyl alcohol.

Mechanical Testing: 180° peel tests (ASTM F2256-05) were performed with a universal testing machine (UTA-500N, Yeonjin) after 5 s of pressing unless otherwise noted. A crosshead speed of 1500 mm min^{-1} after pressing for 5 s at 5 N was used otherwise mentioned. For experiments that evaluated adhesion on wet porcine skin, deionized water was pipetted on the surface prior to testing. For cyclic tensile tests and self-healing measurements (LS-1E, Lloyd), a crosshead speed of 300 mm min^{-1} after pressing for 5 s at 5 N was used, with no rest periods between consecutive cycles. Between consecutive cycles, a layer of interfacial water was maintained on the tissue surface by directing a humidifier to the surface of the porcine skin. The tissue surface was not cleaned between test cycles. When testing the duration of PSB application, a crosshead speed of 2000 mm min^{-1} was used and detachment was visually confirmed. For the mechanical testing of blood covered porcine skin, defibrinated sheep blood was obtained from KisanBio. During cyclic underwater testing, a crosshead speed of 300 mm min^{-1} after pressing for 3 s at 1 N was used.

Interfacial Water Absorption Imaging: Interfacial water absorption was evaluated by attaching PSB or control VHB tape samples to a 2 wt% agarose hydrogel loaded with rhodamine-dye for 2 h. The interface was nondestructively imaged by taking consecutive z-stack images through the hydrogel-tape interface using a confocal microscope. The acquired images were projected on the x or y axis to visualize the rhodamine-dye diffusion as a measure of interfacial water transport and thresholded to the same intensity to find the hydrogel-tape interface.

In Vitro Biodegradability: In vitro biodegradability of the PSB was evaluated by incubation in phosphate-buffered saline (PBS) at 37 °C. To visualize the degradation, the PSB samples (10 mm in width and 10 mm in length, ≈1 g) were attached to slide glasses and immersed in 50 mL conical tubes filled with 50 mL PBS. Then, the conical tubes were placed horizontally and incubated in an incubator at 37 °C (WB-6, Daihan Scientific Co., Ltd). Samples were collected after 0, 0.5, 1, 2, 4, 10, 25, and 50 h and dried in an oven at 65 °C for 24 h. The weight loss of the samples was calculated based on the following equation:

$$\text{Weight ratio } (\%) = \frac{(W_0 - W_d)}{W_0} \times 100 \quad (2)$$

where W_0 was the initial weight of the PSB sample in the dry state and W_d was the degraded weight of the PSB sample in the dry state.

In Vitro Cell Viability: In vitro cell viability was evaluated by a LIVE/DEAD assay based on the PBS-conditioned cell culture media. Control cell culture medium was prepared with 10% of fetal bovine serum (Gibco) and 1% of penicillin-streptomycin (Sigma-Aldrich) in Dulbecco's modified Eagle medium (DMEM). The PSB-conditioned cell culture medium was made by incubating 80 mg of the PSB in 4 mL of the cell culture medium and neutralizing its pH to 7. HEK 293 cells and 3T3 cells were plated on 96-well plates with a control cell culture medium at 37 °C for 24 h in 5% CO_2. The biodegraded PSB-conditioned cell culture medium was prepared using methods similar to those for the PSB-conditioned medium, but with 7 days of embedding time in cell culture medium to ensure complete biodegradation of the PSB. The plated cells were then incubated with the PSB-conditioned, and biodegraded PSB-conditioned cell culture medium at 37 °C for 24 h in 5% CO_2. In vitro cell viability was measured by a LIVE/DEAD viability/cytotoxicity kit for mammalian cells (L3224, Thermo Fisher Scientific). Solution with calcein-AM 5 µL and ethidium homodimer-1 20 µL in 10 mL DPBS (Dulbecco's phosphate-buffered saline) was used for LIVE/DEAD cell staining. Images were collected using a fluorescence microscope. The cell viability result was calculated by a microplate reader (SpectraMax iD3, Molecular Devices) using excitation/emission wavelengths of 485/530 nm and 530/645 nm for live cells and dead cells, respectively.

Vertebrate Animal Subjects: Female Sprague Dawley rats (225 – 250 g, 12 weeks, Koatec) and minipigs (originated from Korean Jeju Island's native pig, 23 – 25 kg, 6 months, Cronex) were used in this work. All rat studies were reviewed and approved by the Korea Advanced Institute of Science and Technology (KAIST) Institutional Animal Care and Use Committee (KA2021-035, KA2022-084, and KA2024-057). All porcine studies were reviewed and approved by the CRONEX Institutional Animal Care and Use Committee.

In Vivo Biocompatibility: In vivo biocompatibility of the PSB was evaluated based on dorsal subcutaneous and epidermal implantation for 1 week. The PSB samples were prepared with styrene-ethylene-butylene-styrene or Ecoflex backing instead of polycarbonate to minimize mechanical mismatch with tissues. For subcutaneous implantation, the PSB with SEBS backing and control (SEBS sample without PSB) were cut into 10 mm × 10 mm. For epidermal implantation, the PSB with Ecoflex backing and control (Ecoflex sample without PSB) were cut into 10 mm × 10 mm. Anesthesia was conducted via an isoflurane inhalation (4% for induction, 2% – 3% for maintenance in O2). After anesthesia, hair on the dorsal region was removed. Surgery was continued on the heating pad for temperature control. Then, a 2 cm skin incision was made on the back of the animal. A subcutaneous pocket was made in the incision by blunt dissection scissors. The PSB with SEBS backing or PSB with no backing material was implanted in the subcutaneous pocket with the PSB side facing the inner tissue. The PSB with Ecoflex backing was sutured on the epidermis 2 cm distally. The same implantation procedures were conducted for the control samples. After 7 days postimplantation, the animals were euthanized and the implanted region was harvested. Harvested tissue was washed with PBS and fixed with formalin for 28 h. Fixed tissue was stained with H&E for histological analysis.

In Vivo Rat Epicardial ECG Recording: For in vivo epicardial ECG recording, a PSB with one electrode (10 µm thick stainless-steel foil, MTI Korea) was prepared in the size of 2 mm × 5 mm. The electrode acted as the recording electrode and was connected by silver paste to a tungsten wire. Anesthesia was conducted via an isoflurane inhalation (4% for induction, 2% – 3% for maintenance in O_2). Surgery was continued on the heating pad for temperature control. Endotracheal intubation was performed to connect the animals to a mechanical ventilator. Then, an incision was made to expose the heart. After exposure of the heart, the pericardium was removed by fine forceps. The PSB with electrode was applied to the epicardial surface for ECG recordings. During the ECG recording, the device was repositioned two times until the desired ECG waveform was recorded.

In Vivo Rat Lung Stabilization: For in vivo lung stabilization, a PSB was attached to a silicon tubing (I.D. 1.5 mm, O.D. 2.5 mm, DAIHAN Scientific). The silicon tubing acted as the vacuum tubing for stabilizing tissue with negative pressure and was connected to mini pump (ZR370-02PM, adafruit). Anesthesia was conducted via an isoflurane inhalation (4% for induction, 2% – 3% for maintenance in O_2). Surgery was continued on the heating pad for temperature control. Endotracheal intubation was performed to connect the animals to a mechanical ventilator. Then, an incision was made to expose the lung. After exposure of the lung, the PSB attached tubing was applied to the lung surface for stabilization.

In Vivo Rat Sciatic Nerve Stimulation: For in vivo sciatic nerve stimulation, a PSB with two electrodes (10 µm thick stainless-steel foil, MTI Korea) was prepared in the size of 1 mm × 2 mm similar to the ECG recording device. Anesthesia was conducted via an isoflurane inhalation (4% for induction, 2% – 3% for maintenance in O_2). Surgery was continued on the heating pad for temperature control. The sciatic nerve was exposed by

dissecting the vastus lateralis muscle and biceps femoris muscle of the animal. The PSB with electrodes was applied to the sciatic nerve. During the sciatic nerve stimulation, the device was repositioned two times to different locations to stimulate diverse sciatic nerve bundles. Biphasic current pulses (1 Hz, 50 μA) were used to stimulate the sciatic nerve.

In Vivo Porcine Epicardial ECG Recording: The minipigs were intubated and anesthetized via inhalation of a 3% isoflurane–oxygen mixture, and placed in a supine position. The minipigs were monitored throughout the entire procedure with ECG and oxygen saturation during entire procedures. To expose the heart and surrounding lungs of the minipig, the left ribs (numbers 6 – 8) were spread as far apart as possible, and the 7th rib was removed. The PSB with two electrodes (10 μm thick stainless-steel foil, 2 mm × 10 mm sized, MTI Korea) was placed on a left ventricle of the minipigs, and ECG recording and analysis were conducted and analyzed in the same method as the rat experiments.

In Vivo Porcine Lung Strain Measurement: A strain sensor was fabricated based on the screen printing of an Ecoflex-CNT composite (CNT 2 wt%). A mold was fabricated via laser patterning (Universal VLS 3.50) on a polycarbonate sheet (GFM, 0.1 mm). Ecoflex layers were coated for the insulation of the Ecoflex-CNT composite. Contact pads were electrically connected with insulated copper wires and sealed with epoxy for mechanical stability. Strain sensor impedance was measured with an LCR meter (1 V, 1 kHz, interval 0.5 s), while undergoing mechanical cycling (LS-1E, Lloyd) of various degrees of strain (1%, 3%, 5%) to verify strain measurement. The PSB with a strain sensor was placed on the left lung lobe surface, and the electrode was then removed and reattached to the area around the lung lobe surface where it was first attached, measured, and then removed and reattached two times. During in vivo porcine testing, strain sensor impedance was measured with an LCR meter (1 V, 1 kHz, interval 0.5 s) and the breathing rate was controlled by a ventilator connected via endotracheal intubation.

Statistical Analysis: OriginPro was used for all statistical data analysis. Data distribution normality was confirmed with Shapiro–Wilk normality tests and homogeneity of variance was confirmed with an F-test between two sample groups. Data were tested to be normal for all data distributions. If homogeneity of variance was confirmed, a two-sample *t*-test was utilized to compare the two groups. Otherwise, Welch's *t*-test was used to compare the two groups.

Supporting Information

Supporting Information is available from the Wiley Online Library or from the author.

Acknowledgements

K.N., Y.K., G.P., and K.H. contributed equally to this work. K.SN. led the investigation on the adhesion mechanism of wet tissue adhesion and their application in in vivo bioelectronics. Y.K. led the investigation on the in vivo tissue stabilization and biocompatibility (in vivo and in vitro) assessment of the PSB. G.P. led the investigation on the material formulation of the PSB. K.H. led the investigation on the chemical characterization and processing of the synthesized PSB. K.N., Y.K., G.P., K.H., J.M.K., Y.L., and S.P. conceptualized the pressure sensitive bioadhesive. K.N., Y.K., G.P., K.H., M.K., and Y.H.L. performed the chemical synthesis of the PSB. K.N, G.P., J.Y.C., C.P., H.L., and J.K. performed rheological characterization and analysis of the PSB. K.N., Y.K., K.H., and J.W.C. performed chemical characterization of the PSB. K.N., Y.K., K.H., D.K., and S.K. performed and analyzed mechanical testing for evaluation of the PSB. Y.K., K.H., C.Y., and S.O. performed in vitro viability and degradation experiments. K.N. and Y.K. performed in vivo biocompatibility and in vivo rat experiments. K.N., Y.K., K.H., J.J., J.R., and J.H, performed in vivo porcine experiments. K.N., Y.K., K.H., and H.Y. contributed to visualization during manuscript drafting. K.N., Y.K., K.H., and S.P. conducted original draft writing. K.N., Y.K., G.P., K.H., J.K., J.H., Y.L., H.Y., and S.P. conducted review & editing. Y.L., H.Y., and S.P. supervised this work. All authors reviewed and approved the submitted manuscript. The authors thanked Dr. Yongsuk Hur at KAIST Biomedical Research Center EM & Histology Core Facility for assistance during histology experiments. Funding: This work was supported by National R&D Program through the National Research Foundation of Korea (NRF) funded by the Ministry of Science and ICT ((Nos. 2022M3H4A1A0409817 and RS-2023-00302489). Figures 1b, 4a,b, 5a,c were created with BioRender.com.

Conflict of Interest

H.Y. has a financial interest in SanaHeal, Inc., a biotechnology company focused on the development of medical devices for surgical sealing and repair. J.M.K. has been a paid consultant and or equity holder for multiple biotechnology companies (listed here https://www.karplab.net/team/jeff-karp). Y.L. has been a paid consultant and or equity holder for AltrixBio inc. and One Fun inc. The interests of J.M.K. and Y.L. were reviewed and are subject to a management plan overseen by their institutions in accordance with their conflict of interest policies.

Data Availability Statement

The data that support the findings of this study are available from the corresponding author upon reasonable request.

Keywords

pressure-sensitive adhesives, surgical adhesives, tissue adhesives

Received: May 19, 2024
Revised: July 20, 2024
Published online:

[1] D. M. Fitzgerald, Y. L. Colson, M. W. Grinstaff, *Nat. Rev. Mater.* **2023**, *8*, 3.
[2] C. Creton, *MRS Bull.* **2003**, *28*, 434.
[3] A. B. Croll, N. Hosseini, M. D. Bartlett, *Adv. Mater. Technol.* **2019**, *4*, 1900193.
[4] M. Sun, N. Kumar, A. Dhinojwala, H. King, *Proc. Natl. Acad. Sci. USA* **2021**, *118*, 2104975118.
[5] M. Li, W. Li, Q. Guan, X. Dai, J. Lv, Z. Xia, W. Ong, E. Saiz, X. Hou, *ACS Nano* **2021**, *15*, 19194.
[6] G. M. Taboada, K. Yang, M. J. N. Pereira, S. S. Liu, Y. Hu, J. M. Karp, N. Artzi, Y. Lee, *Nat. Rev. Mater.* **2020**, *5*, 310.
[7] S. Rose, A. Prevoteau, P. Elzière, D. Hourdet, A. Marcellan, L. Leibler, *Nature* **2014**, *505*, 382.
[8] N. Lang, M. J. Pereira, Y. Lee, I. Friehs, N. V. Vasilyev, E. N. Feins, K. Ablasser, E. D. O'Cearbhaill, C. Xu, A. Fabozzo, R. Padera, S. Wasserman, F. Freudenthal, L. S. Ferreira, R. Langer, J. M. Karp, P. J. del Nido, *Sci. Transl. Med.* **2014**, *6*, 218ra216.
[9] N. Annabi, Y. Zhang, A. Assmann, E. S. Sani, G. Cheng, A. D. Lassaletta, A. Vegh, B. Dehghani, G. U. Ruiz-Esparza, X. Wang, S. Gangadharan, A. S. Weiss, A. Khademhosseini, *Sci. Transl. Med.* **2017**, *9*, eaai7466.
[10] J. Li, A. D. Celiz, J. Yang, Q. Yang, I. Wamala, W. Whyte, B. R. Seo, N. V. Vasilyev, J. J. Vlassak, Z. Suo, D. J. Mooney, *Science* **2017**, *357*, 378.
[11] J. Yang, R. Bai, Z. Suo, *Adv. Mater.* **2018**, *30*, 1800671.
[12] Y. Wang, K. Jia, C. Xiang, J. Yang, X. Yao, Z. Suo, *ACS Appl Mater Interfaces* **2019**, *11*, 40749.
[13] H. Yuk, C. E. Varela, C. S. Nabzdyk, X. Mao, R. F. Padera, E. T. Roche, X. Zhao, *Nature* **2019**, *575*, 169.
[14] H. Yuk, J. Wu, T. L. Sarrafian, X. Mao, C. E. Varela, E. T. Roche, L. G. Griffiths, C. S. Nabzdyk, X. Zhao, *Nat. Biomed. Eng.* **2021**, *5*, 1131.

[15] Y. Liu, G. Guan, Y. Li, J. Tan, P. Cheng, M. Yang, B. Li, Q. Wang, W. Zhong, K. Mequanint, C. Zhu, M. Xing, *Sci. Adv.* **2022**, *8*, eabm9744.
[16] J. Wu, H. Yuk, T. L. Sarrafian, C. F. Guo, L. G. Griffiths, C. S. Nabzdyk, X. Zhao, *Sci. Transl. Med.* **2022**, *14*, eabh2857.
[17] A. H. C. Anthis, M. P. Abundo, A. L. Neuer, E. Tsolaki, J. Rosendorf, T. Rduch, F. H. L. Starsich, B. Weisse, V. Liska, A. A. Schlegel, M. G. Shapiro, I. K. Herrmann, *Nat. Commun.* **2022**, *13*, 7311.
[18] G. Theocharidis, H. Yuk, H. Roh, L. Wang, I. Mezghani, J. Wu, A. Kafanas, M. Contreras, B. Sumpio, Z. Li, E. Wang, L. Chen, C. F. Guo, N. Jayaswal, X. Katopodi, N. Kalavros, C. S. Nabzdyk, I. S. Vlachos, A. Veves, X. Zhao, *Nat. Biomed. Eng.* **2022**, *6*, 1118.
[19] K. Yamagishi, I. Kirino, I. Takahashi, H. Amano, S. Takeoka, Y. Morimoto, T. Fujie, *Nat. Biomed. Eng.* **2019**, *3*, 27.
[20] J. Deng, H. Yuk, J. Wu, C. E. Varela, X. Chen, E. T. Roche, C. F. Guo, X. Zhao, *Nat. Mater.* **2021**, *20*, 229.
[21] Q. Yang, T. Wei, R. T. Yin, M. Wu, Y. Xu, J. Koo, Y. S. Choi, Z. Xie, S. W. Chen, I. Kandela, S. Yao, Y. Deng, R. Avila, T. Liu, W. Bai, Y. Yang, M. Han, Q. Zhang, C. R. Haney, K. B. Lee, K. Aras, T. Wang, M. Seo, H. Luan, S. M. Lee, A. Brikha, N. Ghoreishi-Haack, L. Tran, I. Stepien, F. Aird, et al., *Nat. Mater.* **2021**, *20*, 1559.
[22] S. Nam, B. R. Seo, A. J. Najibi, S. L. McNamara, D. J. Mooney, *Nat. Mater.* **2023**, *22*, 249.
[23] Y. Gao, K. Wu, Z. Suo, *Adv. Mater.* **2019**, *31*, 1806948.
[24] X. Chen, H. Yuk, J. Wu, C. S. Nabzdyk, X. Zhao, *Proc. Natl. Acad. Sci. USA* **2020**, *117*, 15497.
[25] L. K. Borden, A. Gargava, S. R. Raghavan, *Nat. Commun.* **2021**, *12*, 4419.
[26] Y. Zhao, Y. Wu, L. Wang, M. Zhang, X. Chen, M. Liu, J. Fan, J. Liu, F. Zhou, Z. Wang, *Nat. Commun.* **2017**, *8*, 2218.
[27] M. Singh, D. Teodorescu, M. Rowlett, S. Wang, M. Balcells, C. Park, B. Bernardo, S. McGarel, C. Reeves, M. Mehra, X. Zhao, H. Yuk, E. Roche, *Adv. Mater.* **2024**, *36*, 3.
[28] M. Chen, Y. Wu, B. Chen, A. M. Tucker, A. Jagota, S. Yang, *Proc. Natl. Acad. Sci. USA* **2022**, *119*, 2203074119.
[29] B. Xue, J. Gu, L. Li, W. Yu, S. Yin, M. Qin, Q. Jiang, W. Wang, Y. Cao, *Nat. Commun.* **2021**, *12*, 7156.
[30] Y. Wang, G. A. Ameer, B. J. Sheppard, R. Langer, *Nat. Biotechnol.* **2002**, *20*, 602.
[31] A. Patel, A. K. Gaharwar, G. Iviglia, H. Zhang, S. Mukundan, S. M. Mihaila, D. Demarchi, A. Khademhosseini, *Biomater* **2013**, *34*, 3970.
[32] G. Ozturk, A. Pasquale, T. Long, *J. Adhes.* **2010**, *86*, 4.
[33] X. Mao, H. Yuk, X. Zhao, *J. Mech. Phys. Solids* **2020**, *137*, 103863.
[34] E. P. Chang, *J. Adhes.* **1991**, *34*, 189.
[35] H. Yuk, T. Zhang, S. Lin, G. A. Parada, X. Zhao, *Nat. Mater.* **2016**, *15*, 190.
[36] C. Creton, J. Hooker, K. R. Shull, *Langmuir* **2001**, *17*, 4948.
[37] C. Creton, M. Ciccotti, *Rep. Prog. Phys.* **2016**, *79*, 046601.
[38] C. Gay, *Integr. Comp. Biol.* **2002**, *42*, 1123.
[39] K. Brown, J. C. Hooker, C. Creton, *Macromol. Mater. Eng.* **2002**, *287*, 163.
[40] I. Mohammed, M. Charalambides, A. Kinloch, *J. Nonnewton Fluid Mech.* **2015**, *222*, 141.
[41] J. Williams, J. Kauzlarich, *J. Adhes.* **2012**, *88*, 10.
[42] Y. Muranishi, T. Sato, Y. Ueda, Y. Yutaka, Y. Sakaguchi, T. Nakamura, H. Date, *J. Thorac. Dis.* **2018**, *10*, 1081.
[43] S. Tokunaga, C. A. Prejean, G. L. Kay, *J. Thorac. Cardiovasc. Surg.* **2000**, *48*, 489.
[44] Y. Muranishi, T. Sato, Y. Yutaka, Y. Sakaguch, T. Komatsu, A. Yoshizawa, M. Hirata, T. Nakamura, H. Date, *Surg. Endosc.* **2017**, *31*, 4260.
[45] N. Sreeram, E. C. Cheriex, J. L. R. M. Smeets, A. P. Gorgels, H. J. J Wellens, *Am. J. Cardiol.* **1994**, *73*, 298.
[46] C. Sung, W. Jeon, K. Nam, Y. Kim, H. Butt, S. Park, *J. Mater. Chem. B* **2020**, *8*, 6624.
[47] S. Verdier-Sévrain, F. Bonté, *J. Cosmet. Dermatol.* **2007**, *6*, 75.
[48] H. H. Mitchell, T. S. Hamilton, F. R. Steggerda, H. W. Bean, *J. Biol. Chem.* **1945**, *158*, 625.
[49] M. Aleemardani, L. Johnson, M. Z. Trikić, N. H. Green, F. Claeyssens, *Mater. Today Adv.* **2023**, *19*, 100410.
[50] D. H. Lau, C. Clausen, E. A. Sosunov, I. N. Shlapakova, E. P. Anyukhovsky, P. Danilo Jr, T. S. Rosen, C. Kelly, H. S. Duffy, M. J. Szabolcs, M. Chen, R. B. Robinson, J. Lu, S. Kumari, I. S. Cohen, M. R. Rosen, *Circulation* **2009**, *119*, 19.
[51] L. Harrison, R. E. Ideker, W. M. Smith, G. J. Klein, J. Kasell, A. G. Wallace, J. J. Gallagher, *Pacing Clin. Electrophysiol.* **1980**, *3*, 531.
[52] A. D. Kaye, S. Ridgell, E. S. Alpaugh, A. Mouhaffel, A. J. Kaye, E. M. Cornett, A. A. Chami, R. Shah, B. M. Dixon, O. Viswanath, I. Urits, A. N. Edinoff, R. D. Urman, *Pain Ther.* **2021**, *10*, 961.
[53] L. Sperling, *Introduction to Physical Polymer Science*, John Wiley & Sons, New Jersey **2005**.